

## Resistance and dopant profiling along freestanding GaAs nanowires

Stefan Korte, Matthias Steidl, Werner Prost, Vasily Cherepanov, Bert Voigtländer, Weihong Zhao, Peter Kleinschmidt, and Thomas Hannappel

Citation: [Applied Physics Letters](#) **103**, 143104 (2013); doi: 10.1063/1.4823547

View online: <http://dx.doi.org/10.1063/1.4823547>

View Table of Contents: <http://scitation.aip.org/content/aip/journal/apl/103/14?ver=pdfcov>

Published by the [AIP Publishing](#)

---

### Articles you may be interested in

[Polarity driven simultaneous growth of free-standing and lateral GaAsP epitaxial nanowires on GaAs \(001\) substrate](#)

Appl. Phys. Lett. **103**, 223104 (2013); 10.1063/1.4834377

[High-amplitude dynamics of nanoelectromechanical systems fabricated on the basis of GaAs/AlGaAs heterostructures](#)

Appl. Phys. Lett. **103**, 131905 (2013); 10.1063/1.4821920

[Scanning tunneling microscopy with InAs nanowire tips](#)

Appl. Phys. Lett. **101**, 243101 (2012); 10.1063/1.4769450

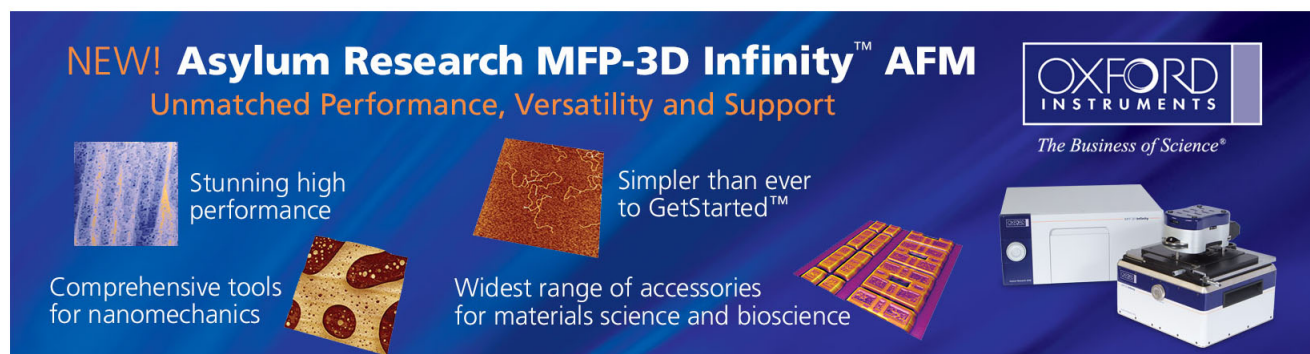
[Size, composition, and doping effects on In\(Ga\)As nanowire/Si tunnel diodes probed by conductive atomic force microscopy](#)

Appl. Phys. Lett. **101**, 233102 (2012); 10.1063/1.4768001

[Incorporation of the dopants Si and Be into GaAs nanowires](#)

Appl. Phys. Lett. **96**, 193104 (2010); 10.1063/1.3428358

---

This is a promotional banner for the Asylum Research MFP-3D Infinity AFM. The background is a deep blue gradient. On the left, the text 'NEW! Asylum Research MFP-3D Infinity™ AFM' is written in white and orange, followed by 'Unmatched Performance, Versatility and Support' in orange. Below this, there are four small images with accompanying text: 1) A blue textured surface with the text 'Stunning high performance'. 2) A brown textured surface with the text 'Simpler than ever to GetStarted™'. 3) A yellow and red patterned surface with the text 'Comprehensive tools for nanomechanics'. 4) A collection of small, colorful rectangular samples with the text 'Widest range of accessories for materials science and bioscience'. On the right side of the banner, the 'OXFORD INSTRUMENTS' logo is displayed in white, with the tagline 'The Business of Science®' underneath. Below the logo is a photograph of the MFP-3D Infinity AFM instrument, which is a white and blue boxy device with a sample stage on top.

# Resistance and dopant profiling along freestanding GaAs nanowires

Stefan Korte,<sup>1</sup> Matthias Steidl,<sup>2</sup> Werner Prost,<sup>3</sup> Vasily Cherepanov,<sup>1</sup> Bert Voigtländer,<sup>1</sup> Weihong Zhao,<sup>2</sup> Peter Kleinschmidt,<sup>2</sup> and Thomas Hannappel<sup>2</sup>

<sup>1</sup>Peter Grünberg Institut (PGI-3) and JARA-Fundamentals of Future Information Technology, Forschungszentrum Jülich, 52425 Jülich, Germany

<sup>2</sup>Photovoltaics Group, Institute for Physics, Technische Universität Ilmenau, 98684 Ilmenau, Germany

<sup>3</sup>CeNIDE and Center for Semiconductor Technology and Optoelectronics, University of Duisburg-Essen, 47057 Duisburg, Germany

(Received 15 July 2013; accepted 13 September 2013; published online 30 September 2013)

Resistance profiles along as-grown GaAs nanowires were measured with a multi-tip scanning tunneling microscope used as a nanoprobe. The nanowires were grown in the vapor-liquid-solid growth mode in a two-temperature-step mode and doped with Zn. Using a transport model, the resistance profile was converted to a dopant profile. The dopant distribution along the nanowires was found to correlate with the temperature during different phases of nanowire growth. The nanowire base grown at higher temperature exhibits a decreased dopant concentration. Mechanical stress by intentional bending of a nanowire was shown not to influence nanowire conductance. © 2013 AIP Publishing LLC. [<http://dx.doi.org/10.1063/1.4823547>]

III–V nanowires (NWs) could form the basis of future nanoscale electronic and optoelectronic devices. Their specific one-dimensional NW geometry enables new device concepts allowing, i.e., all-around gate control in FETs,<sup>1</sup> resonant light trapping in solar cells,<sup>2</sup> or new radial structures allowing for ultra-high efficiencies, even with low minority carrier diffusion lengths.<sup>3</sup> For the fabrication of novel high performance NW devices a precise control of doping density and doping profile is indispensable. However, a precise doping control is often difficult to obtain.<sup>4</sup> For instance, the growth of NWs can require procedures such as two-step growth, using first high temperature to initiate straight, epitaxial growth, and subsequently lower temperature to obtain untapered wires without twin defects.<sup>5</sup> This two step growth process with varying temperatures is expected to influence dopant incorporation into the NWs strongly. Moreover, the determination of the local resistivity and transport data in NWs is difficult to obtain due to the nanoscaled one-dimensional geometry. In most cases of previous measurements the NWs were detached from the surface and specific test devices based on ultra-high precision lithography, such as FETs,<sup>6,7</sup> transmission lines,<sup>4</sup> or even Hall patterns,<sup>8</sup> were fabricated. Alternatively, nanoprobe and multi-tip scanning tunneling microscopes (STM) can be used to investigate the resistance along a single NW, because they allow flexible placement of up to four contacts on a single NW, as done, e.g., on flat-lying SnO<sub>2</sub> NWs placed on SiO<sub>2</sub>.<sup>9</sup> To better explore NW functionality for future devices it is advantageous to measure the electrical properties on free-standing NWs directly while they are still attached to the substrate. This approach was followed with two point measurements<sup>10</sup> as well as four probe measurements.<sup>11</sup> However, no resistance profiling was performed in these measurements.

In this work we use a multi tip STM as nanoprobe to contact as-grown, freestanding NWs, as shown in Figs. 1(a) and 1(b). This enabled us to measure a continuous resistance profile and, subsequently, to obtain the dopant profile along the length of a wire using resistance model calculations.<sup>12</sup>

GaAs NWs with diameters between 50 and 150 nm had previously been found to bend elastically up to a strain limit of 10%–11%.<sup>13,14</sup> So we were able to use a nanoprobe tip to bend a freestanding NW and measure its resistance in the presence of mechanical stress.

GaAs NWs as the ones shown in Fig. 1(a) were grown on *n*-type GaP(111)B substrates by metal-organic vapor phase epitaxy (MOVPE) in an AIX200 RF system with an entirely non-gaseous source configuration.<sup>12</sup> As growth seeds mono-disperse Au-particles with a diameter of 100 nm were deposited from a colloidal solution. Prior to the NW growth two steps were carried out. First, the substrate was annealed at 600 °C for 10 min under group V overpressure provided by tertiary butyl phosphine (TBP) in order to clean the substrate and to generate an eutectic melt by diffusion of Ga into the Au-particles. Next, the temperature was reduced to 450 °C and diethyl zinc (DEZn) was offered for 4 min in order to pre-saturate the Au-particle with Zn. The subsequent NW growth

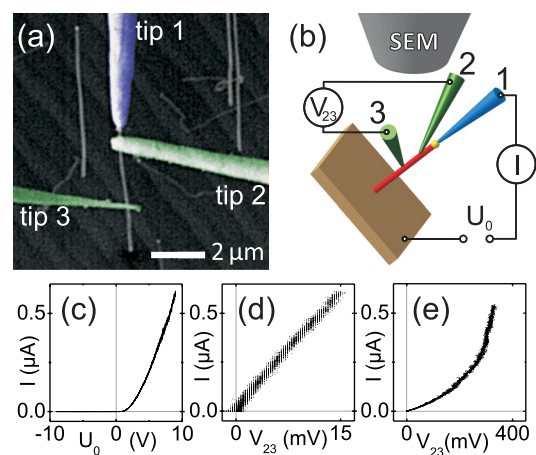


FIG. 1. (a) SEM image of a freestanding GaAs NW contacted with three tips. The sample is tilted by 45°. (b) Schematic diagram including the wiring for four point resistance measurements on the NW. A typical two point I–V measurement is shown in (c), as well as four point I–V-curves taken with tip 3 (d) close to tip 2 and (e) close to the NW base.

was carried out with trimethyl gallium (TMGa) and tertiary butyl arsine (TBAs) at a V/III ratio of 2.5 in two temperature steps.<sup>5</sup> The DEZn flow was kept constant resulting in a dopant to TMGa (II/III ratio) of 0.002. Initially the temperature was set to 450 °C for 3 min, permitting the beginning of the growth of straight, vertically aligned NWs. To reduce tapering and enhance the crystallographic quality of the NWs, the temperature was then lowered to 400 °C, and growth took place for another 30 min. During the whole process the total pressure was 50 millibars with a total gas flow of 3.4 l/min, which was provided by N<sub>2</sub> as the main carrier gas, while H<sub>2</sub> was used for the sources. The average length of our NWs grown this way was  $l \approx 8.2 \mu\text{m}$ , their diameter  $2r \approx 125 \text{ nm}$  in the 450 °C region, and their diameter along the 400 °C regime was reaching from  $2r \approx 115 \text{ nm}$  at the bottom to 95 nm below the Au-droplet, determined by high resolution SEM. This corresponds to a tapering of  $\Delta r/\Delta l < 0.2\%$ .

A home-built coaxial beetle-type multitip STM<sup>15</sup> in combination with an SEM column was used to conduct four point electrical measurements on the as-grown NWs. The sample was mounted with a 45° tilt, so that the NWs could be observed by SEM and three electrochemically etched tungsten tips could be brought into contact with the same NW. Figs. 1(a) and 1(b) show a NW contacted by three tips. The *n*-GaP substrate is used as additional fourth contact to the NW allowing for four-point electrical measurements to evaluate the conductance of the NW without the influence of contact resistances. Tip 1 contacted a NW at the Au seed particle on top, in order to inject and measure the electrical current  $I$  through the NW into the sample. Due to the *p*-*n* junction between the *p*-doped NW and the *n*-doped substrate, a measurable current flows in forward direction, only (Fig. 1(c)). Typically, a current up to 1  $\mu\text{A}$  was employed, because significantly higher currents resulted in melting the NWs. During the four point measurements tips 2 and 3 contacted the NW along its length and measured the potentials  $V_2$  and  $V_3$  and thus the voltage drop  $V_{23} = V_2 - V_3$  that occurred in between the contact points along the NW (Figs. 1(b) and 2(a)). From the slope of the resulting  $I$  versus  $V_{23}$  curves, the resistance  $R_{23}$  of the NW segment between the voltage probe tips was calculated by a linear fit, excluding any influence of contact resistances between tips and NW. The contact resistance for tip 1 contacting the Au particle was usually in the range of a few k $\Omega$ , those of tips 2 and 3 varied and could be up to some 100 M $\Omega$ .

In order to obtain a resistance profile along a NW as shown in Fig. 2(b) (black points), the position of tip 3 was moved along the NW in between different resistance measurements, while tip 2 was always kept at the same position near the top of the NW. Other NWs from the same preparation showed similar profiles. Most of the NW length shows a linear resistance increase of 12 k $\Omega/\mu\text{m}$ , corresponding to a constant resistivity, in good agreement with the results obtained on lithographically contacted GaAs NWs with similar composition.<sup>12</sup> However, due to the high spatial resolution of our method we observed a previously undetected sharp rise of the resistivity, to a linear resistance increase of 20 M $\Omega/\mu\text{m}$  at the NW base, where the temperature during NW growth was higher (Fig. 2(a)). This part of the resistance profile is shown with a logarithmic scale for better visibility

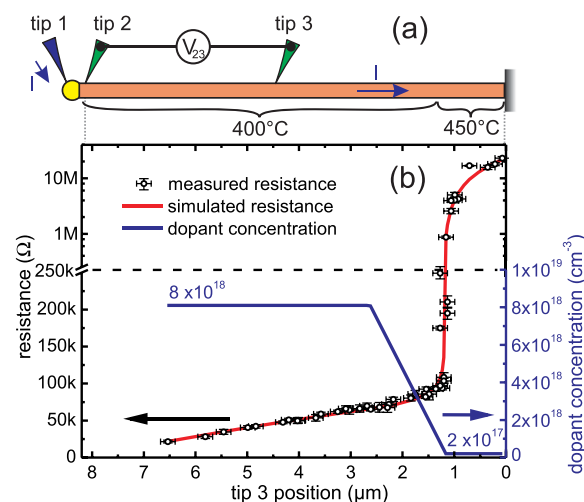


FIG. 2. (a) Schematic illustration of a four point measurement on a NW performed in order to obtain the resistance of the NW segment between tip 2 and tip 3. Also the growth temperature for different parts of the NW is given. (b) The resistance profile of a GaAs NW from top to base (black points), as well as the modeled resistance profile (red line) and the dopant concentration (blue line, right axis) used to model the data. Above the dashed line the resistance scale is logarithmic in order to display the resistance profile of the NW base properly. The resistance increases linear in this region.

in Fig. 2(b). This part of the NWs is not easily accessible by lithographic contact methods, while the nanoprobe allows four point measurements at the NW base down to distances from the substrate corresponding to the tip radius, which can be 50 nm or smaller. The increased resistivity at the base may dominate future NW devices contacted via a conductive substrate and deserves additional investigation. While the NWs exhibited linear  $I(V_{23})$  characteristics along most of their length (Fig. 1(d)), these curves showed increasingly nonlinear characteristics when tip 3 approaches the NW base (Fig. 1(e)). We attribute this to Joule heating due to the higher resistivity in this NW part. In this case the fit range to obtain the NW resistance was reduced to the linear part of the  $I(V_{23})$  curves at low current (e.g., up to 30 mV for the curve shown in Fig. 1(e)). Up to eight  $I(V_{23})$  curves were evaluated for each position to assess the spread of the resistance measurements, ranging from 1% to 11%, depending on the contact conditions. The tip position determination using SEM was estimated to have an accuracy of  $\pm 140 \text{ nm}$ .

The measured variation of the resistance profile along the NW is attributed to a variation of dopant density  $N_A$  along the wire.<sup>4,12</sup> As we are not able to evaluate the radial distribution of the dopant density, the model is restricted to an average density across the NW diameter. This assumption neglects a possible radial distribution due to a vapor-liquid-solid growth based doping mechanism in the core and due to the different layered growth based mechanism for the tapered shell. Especially the latter aspect may play an important role in case of highly tapered NWs which are avoided in this work. In the following the measured resistance profile is described using a transport model which takes the geometrical data into account (radius  $r(l)$  along the NW, and the contact positions  $l_2$  and  $l_3$  of tips 2 and 3). Also the GaAs surface depletion length  $d_{spc}$  caused by a surface potential of  $\varphi_s = 0.5 \text{ V}$ , and a doping density dependent mobility  $\mu(N_A)$  are included.<sup>12</sup> This model results in a resistance  $R_{23}$  as



$$R_{23} = \int_{l_2}^{l_3} \frac{1}{qN_A(l) \times \mu(N_A(l))} \times \frac{\delta l}{\pi(r(l) - d_{spc}(N_A(l)))^2} \quad (1)$$

Since the resistance  $R_{23}$  increases almost linearly both in the NW part between  $6.5 \mu\text{m}$  and  $2.5 \mu\text{m}$  grown at  $400^\circ\text{C}$  and also in the base ( $1.2 \mu\text{m}$  to  $0 \mu\text{m}$ , grown at  $450^\circ\text{C}$ ), we assume a constant dopant concentration in both regions (Fig. 2(b), blue line). Fitting the model data (Eq. (1)) within the NW part grown at  $450^\circ\text{C}$  yields a dopant concentration of  $N_{A,450^\circ\text{C}} = 2 \times 10^{17} \text{ cm}^{-3}$ . For the  $400^\circ\text{C}$  region, one obtains a good fit for  $N_{A,400^\circ\text{C}} = 8 \times 10^{18} \text{ cm}^{-3}$ . The low Zn-incorporation at  $450^\circ\text{C}$  can be explained by an improved pyrolysis yield of TMGa compared to  $400^\circ\text{C}$ . While DEZn already completely pyrolyzes at  $400^\circ\text{C}$ ,<sup>16</sup> around 5% of TMGa decompose at  $400^\circ\text{C}$  and 30% at  $450^\circ\text{C}$ .<sup>17</sup> Thus, the effective II/III ratio is expected to be much higher at  $400^\circ\text{C}$  than at  $450^\circ\text{C}$ . The resistance profile is not linear in the region of the NW grown immediately after the growth temperature was lowered ( $1.2 \mu\text{m}$  to  $2.5 \mu\text{m}$ ). We assume here as a first order approximation a linear dopant increase between  $N_{A,450^\circ\text{C}}$  and  $N_{A,400^\circ\text{C}}$  towards lower growth temperatures (Fig. 2(b)). It should be mentioned that choosing the transition length from  $1.0 \mu\text{m} < l_T < 1.8 \mu\text{m}$  after the point of temperature decrease still yields acceptable fits, too. Altogether, the calculated resistance profile (red line in Fig. 2(b)) exhibits very good agreement to the measured data (black points) and supports the dopant distribution discussed above. These constant doping concentrations differ from doping gradients over  $10 \mu\text{m}$  found by Gutsche *et al.*,<sup>12</sup> where no Zn was offered before growth. Without pre-saturation of the Zn dopant in the Au seed droplet and, especially at a low DEZn flow, the retarded dopant incorporation in the Au seed particle causes axially extended doping profiles.<sup>18</sup> We reduced these gradients by saturating the Au-particles with Zn dopant before NW growth was initiated.

To explore the influence of NW deformation on its conductivity, the resistance of one NW was compared for straight configuration, similar to Fig. 1(a), and strongly bent configuration as shown in the SEM image Fig. 3(a). To bend the NW, the tip contacting the Au nanoparticle was moved to push the NW towards the substrate. The voltage probe tips were repositioned to contact the strained NW for resistance measurements as shown in the 3-dimensional representation in Fig. 3(b). When the NW was released again, it reverted to a straight configuration, proving an elastic deformation

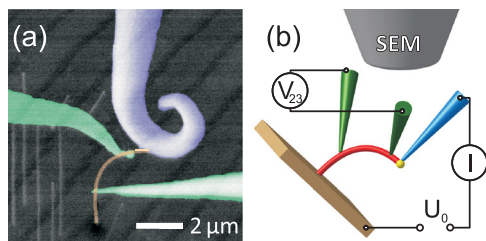


FIG. 3. A NW (orange) is strongly bent by the uppermost tip (blue, curled up from previous experiments) and contacted for resistance measurement. No significant change in NW resistance compared to a straight configuration was observed.

during bending. In the straight configuration, the segment of the NW between the voltage probing tips showed a resistance of  $65.5 \pm 0.2 \text{ k}\Omega$ . The bent NW gave resistances between  $55 \text{ k}\Omega$  and  $75 \text{ k}\Omega$ . This sets an upper boundary of  $\pm 15\%$  for the effect of mechanical stress on the conductivity, despite the strong NW bending performed. However, we attribute this spread mostly to uncertainties in the distance between tips 2 and 3 when reproducing the contact positions along the bent NW due to the curvature of the NW and the two-dimensional projection in SEM view.

In summary, we have used a multi-tip STM as a nano-prober to measure the resistance profile of freestanding GaAs NWs with high accuracy. Conversion of the resistance profile to a dopant profile via a transport model displayed a reduced incorporation of dopants into the NW base. The reduced doping is most probably caused by the higher temperature during the beginning of the two-temperature mode NW growth, applied to enhance vertical alignment of the NWs, and has to be considered when building devices from freestanding NWs contacted via the substrate. The dependence of NW conductance on strain in a severely bent NW was explored. In our experiments, mechanical stress on a NW during four point probe measurements was shown not to influence its electrical conductance.

The authors are indebted to H. P. Bochem for taking high resolution SEM images for NW diameter determination. Funding by the German federal ministry of education and research and of environmental protection and reactor safety within the project “nano-III/V-pin’s” of the photovoltaic innovation alliance (BMBF, Project No. 03SF0404A) is gratefully acknowledged.

<sup>1</sup>T. Bryllert, L.-E. Wernersson, L. E. Froberg, and L. Samuelson, *IEEE Electron Device Lett.* **27**, 323 (2006).

<sup>2</sup>J. Wallentin, N. Anttu, D. Asoli, M. Huffman, I. Aberg, M. H. Magnusson, G. Siefert, P. Fuss-Kailuweit, F. Dimroth, B. Witzigmann, H. Q. Xu, L. Samuelson, K. Deppert, and M. T. Borgstrom, *Science* **339**, 1057 (2013).

<sup>3</sup>B. M. Kayes, H. A. Atwater, and N. S. Lewis, *J. Appl. Phys.* **97**, 114302 (2005).

<sup>4</sup>C. Gutsche, A. Lysov, I. Regolin, K. Blekker, W. Prost, and F.-J. Tegude, *Nanoscale Res. Lett.* **6**, 65 (2011).

<sup>5</sup>H. J. Joyce, Q. Gao, H. H. Tan, C. Jagadish, Y. Kim, X. Zhang, Y. Guo, and J. Zou, *Nano Lett.* **7**, 921 (2007).

<sup>6</sup>W. Prost, K. Blekker, Q.-T. Do, I. Regolin, F.-J. Tegude, S. Müller, D. Stichtenoth, K. Wegener, and C. Ronning, “Modeling the Carrier Mobility in Nanowire Channel FET,” *MRS Proceedings* **1017**, 1017-DD14-06 (2007).

<sup>7</sup>S. Dayeh, D. P. Aplin, X. Zhou, P. K. Yu, E. Yu, and D. Wang, *Small* **3**, 326 (2007).

<sup>8</sup>Ch. Blömers, T. Grap, M. I. Lepsa, J. Moers, St. Trellenkamp, D. Grützmaker, H. Lüth, and Th. Schäpers, *Appl. Phys. Lett.* **101**, 152106 (2012).

<sup>9</sup>C. Ru, Y. Zhang, Y. Sun, Y. Zhong, X. Sun, D. Hoyle and I. Cotton, *IEEE Trans. Nanotechnol.* **10**, 674 (2011).

<sup>10</sup>O. Salehzadeh, M. X. Chen, K. L. Kavanagh, and S. P. Watkins, *Appl. Phys. Lett.* **99**, 182102 (2011).

<sup>11</sup>C. Durand, M. Berthe, Y. Makoudi, J.-P. Nys, R. Leturcq, P. Caroff, and B. Grandidier, *Nanotechnol.* **24**, 275706 (2013).

<sup>12</sup>C. Gutsche, I. Regolin, K. Blekker, A. Lysov, W. Prost, and F. J. Tegude, *J. Appl. Phys.* **105**, 024305 (2009).

<sup>13</sup>P. A. Alekseev, M. S. Dunaevskii, A. V. Stopyaga, M. Lepsa, and A. N. Titkov, *Semiconductors* **46**, 641 (2012).

<sup>14</sup>Y.-B. Wang, L.-F. Wang, H. J. Joyce, Q. Gao, X.-Z. Liao, Y.-W. Mai, H. H. Tan, J. Zou, S. P. Ringer, H.-J. Gao, and C. Jagadish, *Adv. Mater.* **23**, 1356 (2011).

- <sup>15</sup>V. Cherepanov, E. Zubkov, H. Junker, S. Korte, M. Blab, P. Coenen, and B. Voigtländer, [Rev. Sci. Instrum.](#) **83**, 033707 (2012).
- <sup>16</sup>C. Thiandoume, V. Sallet, R. Triboulet, and O. Gorochov, [J. Cryst. Growth](#) **311**, 1411 (2009).
- <sup>17</sup>M. Pristovsek, Ph.D. thesis, Technische Universität Berlin, 2001.
- <sup>18</sup>Influences of Zn diffusion along the NW during growth are expected to play no role, as it is limited to the low nanometer range within the growth temperatures. Inferred from: T. K. Sharma, A. P. Shah, M. R. Gokhale, C. J. Panchal, and B. M. Arora, [Semicond. Sci. Technol.](#) **14**, 327 (1999).